EPJ Web of Conferences **172**, 02004 (2018) https://doi.org/10.1051/epjconf/201817202004
ISMD 2017

Future Measurements of the Nucleon Elastic Electromagnetic Form Factors at Jefferson Lab

Gerard Gilfoyle[1,⋆]

[1] *Physics Department, University of Richmond, Richmond, VA, USA*

Abstract. The elastic, electromagnetic form factors are fundamental observables that describe the internal structure of protons, neutrons, and atomic nuclei. Jefferson Lab in the United States has completed the 12 GeV Upgrade that will open new opportunities to study the form factors. A campaign to measure all four nucleon form factors (electric and magnetic ones for both proton and neutron) has been approved consisting of seven experiments in Halls A, B, and C. The increased energy of the electron beam will extend the range of precision measurements to higher Q^2 for all four form factors together. This combination of measurements will allow for the decomposition of the results into their quark components and guide the development of a QCD-based understanding of nuclei in the non-perturbative regime. I will present more details on the 12 GeV Upgrade, the methods used to measure the form factors, and what we may learn.

1 Introduction

The elastic electromagnetic form factors are fundamental observables in electron scattering that encode information about the distribution of electric charge and current in the nucleus and its constituents. The study of nuclei with electromagnetic probes has a long, distinguished history in nuclear physics including the Nobel Prize awarded to Robert Hofstadter in 1961 [1]. With the completion of the 12 GeV Upgrade at the Thomas Jefferson National Accelerator Facility (JLab) in Newport News, VA, USA we now stand on the doorstep of a new chapter in our understanding of atomic nuclei [2]. The JLab Program Advisory Committee (PAC) has approved a campaign of seven experiments to run in three different experimental halls to measure the elastic, electric and magnetic form factors for both the neutron and proton. The focus of the campaign will be mapping out the quark substructure of the nucleon far beyond our current range and to test the fundamental theory of the strong force, Quantum Chromodynamics (QCD), in the non-perturbative region.

In this paper we present a status report on our current understanding of the elastic, electromagnetic form factors (EEFFs) of the nucleon and what we may learn with the extended reach of this new generation of experiments at JLab. We then describe how that reach will be extended in the JLab campaign. We end with a summary and conclusions.

⋆e-mail: ggilfoyl@richmond.edu

2 Where We Are Now.

In this section we present some of the necessary background to understand the EEFFs and then discuss selected topics in our current experimental and theoretical understanding. The electromagnetic form factors are the essential components of the cross section in the region where the one-photon exchange is applicable. That cross section can be expressed in terms of the Dirac (F_1) and Pauli (F_2) form factors

$$\frac{d\sigma}{d\Omega} = \sigma_{Mott}\left[(F_1^2 + \kappa^2\tau F_2^2) + 2\tau(F_1 + \kappa F_2)^2 \tan^2\left(\frac{\theta_e}{2}\right)\right] \tag{1}$$

where

$$\sigma_{Mott} = \frac{\alpha^2 E' \cos^2(\frac{\theta_e}{2})}{4E^3 \sin^4(\frac{\theta_e}{2})} \tag{2}$$

and κ is the anomalous magnetic moment, E (E') is the incoming (outgoing) electron energy, θ_e is the scattered electron angle and $\tau = Q^2/4M^2$. The Dirac and Pauli form factors can be recast into electric and magnetic parts - the Sachs form factors .

$$\frac{d\sigma}{d\Omega} = \frac{\sigma_{Mott}}{\epsilon(1+\tau)}\left(\epsilon G_E^2 + \tau G_M^2\right) \tag{3}$$

where

$$G_E = F_1 - \kappa\tau F_2 \quad \text{and} \quad G_M = F_1 + \kappa F_2 \quad \text{and} \quad \epsilon = \left[1 + 2(1+\tau)\tan^2\frac{\theta_e}{2}\right]^{-1} \tag{4}$$

There is an extensive data set for the EEFFs at lower 4-momentum transfer squared or Q^2, but the data become sparse at increasing Q^2. The proton magnetic form factor G_M^p has the best data set at this point. Figure 1a shows the world's data for G_M^p relative to the dipole form factor. The dipole form factor is $G_D = (1 + Q^2/\Lambda)^{-2}$ where $\Lambda = 0.71$ GeV^2. The measurements extend out to $Q^2 \approx 30$ GeV^2

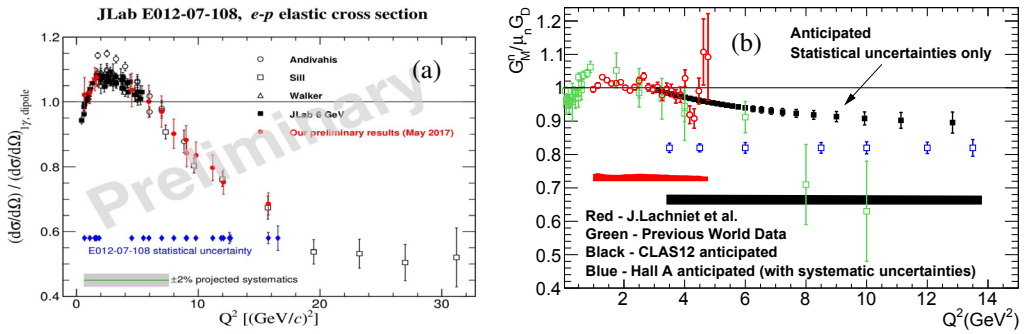

Figure 1. The world's data for $G_M^p/\mu_p G_D$ data are shown in panel (a) [3]. The red points are preliminary results from Experiment E12-07-108. The world's data for $G_M^n/\mu_n G_D$ are shown in panel (b) [4]. The measured points are the green, open squares and the red, open circles. The uncertainties on the red points are statistical ones. The red bar chart represents the systematic uncertainties on the red data points. The other data points are anticipated ones for future experiments and are discussed below.

and are particularly dense for $Q^2 < 8$ GeV^2. Above 8 GeV^2 they are sparse and the uncertainties grow. This is where the JLab program will have the greatest impact. The red points in Figure 1a are preliminary results from JLab experiment E12-07-108 which completed data collection in 2017. The uncertainties on the red points are much larger than what is expected for the final results ($\approx 2\%$). The

more-difficult-to-measure neutron magnetic form factor G_M^n measurements are more limited in Q^2 coverage and are shown in Figure 1b. The measured results are the green, open squares and the red, open circles. The data are precise out to $Q^2 \approx 5$ GeV^2 with a few more points with large uncertainties extending out to $Q^2 = 10$ GeV^2.

The Sachs nucleon electric form factors G_E^p and G_E^n are now routinely shown as the ratio relative to the magnetic form factors $\mu_p G_E/G_M$. The world's data for both proton and neutron ratios are shown in Figure 2. The proton ratio is extracted with the recoil polarization method (which will be discussed

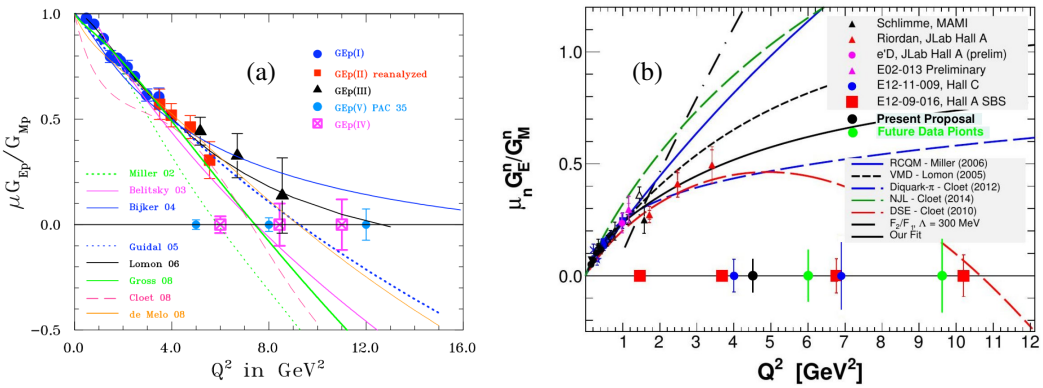

Figure 2. World's data for the proton form factor ratio $\mu_p G_E^p/G_M^p$ data using the recoil polarization method are shown in panel (a) [5, 6]. World's data for $\mu_n G_E^n/G_M^n$ are shown in panel (b) [7]. In both cases the points plotted along the axis represent the anticipated Q^2 and uncertainty on future measurements.

below) and drops linearly from $Q^2 = 0$. The data extend out to $Q^2 \approx 8$ GeV^2. This behavior is in sharp contrast to earlier measurements using the Rosenbluth separation methods which showed a Q^2 dependence largely constant at unity although with large uncertainties [8]. This radical difference is now mostly attributed to two-pion exchange [9]. There also appears to be a zero-crossing around the highest Q^2 point. The significance of this feature is discussed below. The neutron electric form factor data is extracted with both the double-spin asymmetry and the recoil polarization methods (more discussion below). The data here are even more limited. They extend only out to $Q^2 = 3.5$ GeV^2 and are steadily rising. It is worth noting here that many of the measurements discussed above have been made over the last twenty years and have generated renewed interest in the EEFFs especially at large Q^2. We next explore what these new data have revealed and where they may lead.

By measuring all four nucleon EEFF's and invoking charge symmetry the quark Dirac and Pauli form factors can be extracted [10].

$$F^u_{1(2)} = 2F^p_{1(2)} + F^n_{1(2)} \qquad \text{and} \qquad F^d_{1(2)} = 2F^n_{1(2)} + F^p_{1(2)} \tag{5}$$

One can now make a flavor decomposition and determine the Q^2-dependence of the individual valence quarks [11]. The result of this process is shown in Figure 3 [10]. There are large differences between the u- and d-quark distributions both in size and shape. The u-quark form factors in Figure 3 are scaled by Q^4 and still rise steadily across the full range while the d-quark form factors saturate at around $Q^2 = 1.4$ GeV^2. To normalize the two quark distributions to each other at low-Q^2 requires applying factors (0.75 and 2.5 in Figure 3) that differ by more than a factor of three. In addition, the Q^2 dependence of the form factor ratio F_2/F_1 is predicted by perturbative QCD to follow a $1/Q^2$ form (see Figure 1 in Reference [10]). This feature differs sharply from the results in Figure 3 and also

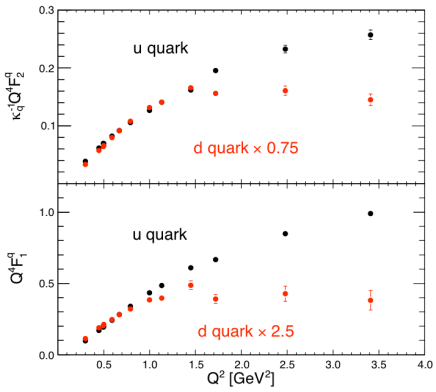

Figure 3. Flavor decomposition of the nucleon elastic form factors showing the Q^2 behavior of the Dirac and Pauli form factors for the $u-$ and $d-$quarks [10]. The form factors are multiplied by Q^4 to show their properties more clearly.

for the behavior of the proton and neutron form factors. A calculation of the flavor form factors has found encouraging agreement with the data using the Nambu-Jona-Lasinio model with the empirical nucleon form factors and treating the pion degrees of freedom as a perturbation on the quark core [12]. The quark form factors are extracted assuming charge symmetry. No model parameters are adjusted to fit the data. Diquark correlations arise naturally in this model and may provide an explanation of the $u-$ and d-quark Q^2 dependence in Figure 3.

Another theoretical approach to describing the EEFFs is shown in Figure 4 which also shows the proton form factor ratio data. The Dyson-Schwinger equations (DSEs) are the equations of motion of quantum field theory and form an infinite set of coupled, integral equations. They are inherently

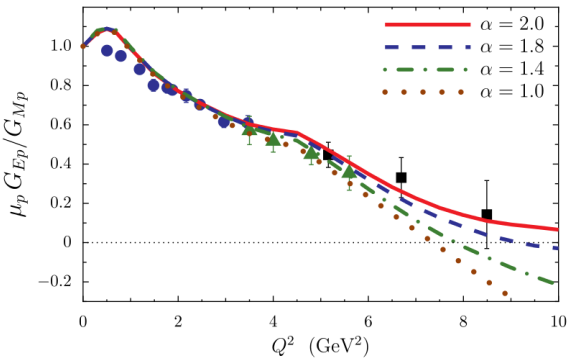

Figure 4. A calculation of the proton form factor ratio $\mu_p G_E^p / G_M^p$ using the Dyson-Schwinger approach[13]. The different curves are linked to different shapes of the mass function $M(p)$ which describes how the proton acquires mass through the dynamical chiral symmetry breaking mechanism.

relativistic, non-perturbative, and deeply connected to QCD. Choosing the proper subset of equations is an essential step in connecting the DSEs to measurement. In Reference [13], Cloët *et al.* model

the nucleon dressed quark operator as a quark-diquark combination and include a damping factor to alter the shape of the momentum dependence of the dressed-quark mass function $M(p)$. This mass function describes how the nucleons acquire mass from dynamical chiral symmetry breaking. The authors calculate the ratio of the proton form factors $\mu_p G_E^p/G_M^p$ and observe a zero crossing in this ratio near the Q^2 limit of the existing data. The different curves shown in Figure 4 are for different values of the damping factor and show how changing the shape of $M(p)$ changes the Q^2 value of the crossover point. In other words, measuring this crossover is revealing how the proton acquires mass. A precise measurement of the the proton form factor ratio at higher Q^2 is needed to determine this crossover.

In the discussion of Figure 3 above it was noted that the data are not well described by perturbative QCD. Another calculation of the quark form factors is described in Reference [14] within the framework of the light-front holographic QCD (LFHQCD). This approach takes advantage of a striking relationship between light-front dynamics, its holographic mapping to gravity in a higher-dimensional anti-de Sitter space, and conformal quantum mechanics [14]. To obtain good agreement with the data an admixture of a five quark state is included in the proton (30%) and the neutron (40%). A third parameter r is introduced to account for $SU(6)$ spin-flavor symmetry breaking and adjusted to fit the data. The results for the neutron form factor ratio $\mu_n G_E^n/G_M^n$ are shown in Panel (a) in Figure 5. The fitted value of $r = 2.08$ is required to produce the green curve which agrees well with the data. The orange curve shows the same calculation with no $SU(6)$ spin-flavor symmetry breaking (*i.e.* $r = 1.0$). Note the calculation (green curve) approaches an asymptotic value at large Q^2. In Panel (b) a

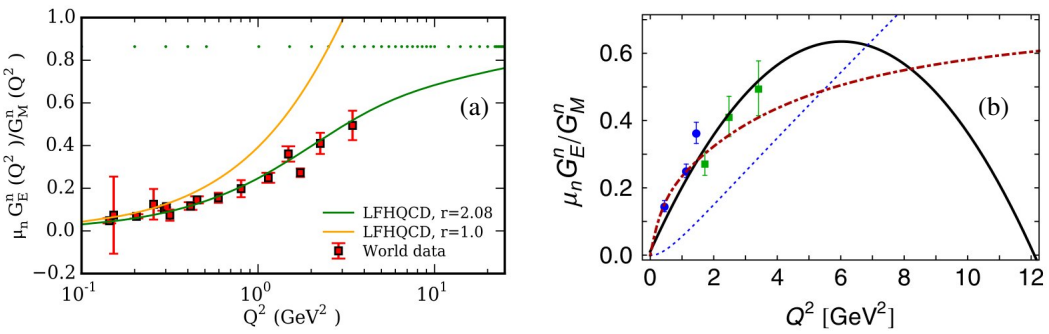

Figure 5. Panel (a) shows the neutron form factor ratio $\mu_n G_E^n/G_M^n$ calculated from the LFHQCD model (green curve) [14]. The model approaches an asymptotic value as $Q^2 \to \infty$ of 0.86 ± 0.11 (green points). Panel (b) shows the result of a calculation using the DSE approach (black curve) [15]. The red, dot-dashed curve is a parameterization of the data [16]. The blue, dashed curve is a contact interaction calculation [17].

prediction of the same ratio using the Dyson-Schwinger approach discussed above is shown [15, 18]. Like a similar calculation of the proton ratio shown in Figure 4 above, it has a zero crossing at high Q^2 where the LFHQCD calculation is approaching its asymptotic value of 0.86 ± 0.11. This zero crossing is a striking difference with the LFHQCD calculation and presents an opportunity to probe fundamental hadronic physics and confinement. Data at higher Q^2 are needed to distinguish between these two calculations.

Lattice QCD calculations are now becoming feasible in the few-GeV^2 range, and over the next decade these calculations will become increasingly precise [19]. The elastic form factors for both the proton and neutron are an important, early test case of the accuracy of the lattice calculations. With all four of them, one can extract the isovector combination of the form factors [20] which are easier

to calculate on the lattice because they lack disconnected contributions [21]. Figure 6 shows a recent calculation. The blue points are the results of the calculation and the red curve is a parameterization of the data. There is excellent agreement between the data parameterization and the calculations, but note the limited Q^2 range - only out to $Q^2 = 1.3$ GeV^2. Higher Q^2 data will continue to challenge these calculations. Finally, Generalized Parton Distributions combine information from the EEFFs

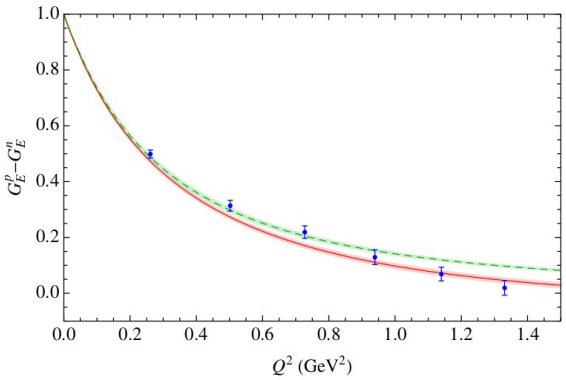

Figure 6. The results of a lattice QCD calculation of the isovector combination of the form factors ($G_E^p - G_E^n$) in shown [22]. The blue points are the calculation and the red curve is a parameterization of the data. The green dashed curve is a fit to the calculated points (blue).

and parton distribution functions (PDFs) and provide a deeper picture of nucleon structure including the role of orbital angular momentum [23]. The elastic form factors are a limiting case of the GPDs and provide an essential constraint on GPD models. We now discuss how those measurements will be made.

3 Where We Are Going

The campaign to measure the EEFFs at JLab begins with CEBAF - a superconducting, continuous-wave, electron accelerator with beams up to 12 GeV, an energy resolution of 2×10^{-4}, and polarization greater than 80%. The 12 GeV Upgrade has recently been completed and the accelerator is now in production running. There are four end stations for experiments (Halls, A, B, C, and D). The EEFF campaign will be carried out in three of those halls (A, B, C). The lineup of approved experiments is shown in Table 1. All of the experiments in the table are based on measurements performed during the earlier 6-GeV era at JLab. More than 200 days of beamtime have been approved to measure the elastic electromagnetic form factors. Details of the experimental program will be given below.

The proton magnetic form factor G_M^p is the best-known of the EEFFs and that understanding will be strengthened by JLab Experiment E12-07-108 in Hall A. A precise measurement of the ep elastic cross will be made using the HRS spectrometers [3]. The range of very precise cross sections will be extended up to $Q^2 = 15$ GeV^2 with expected systematic uncertainties of 2%. Data collection was completed in 2017 and the analysis is underway. Preliminary results (with increased uncertainties) are shown in Figure 1a. This first measurement is crucial because it sets the scale for the remaining EEFF measurements.

The measurement of the proton form factor ratio $\mu_p G_E^p/G_M^p$ (E12-07-109) will also be performed in Hall A using the recoil polarization method on a proton cryo-target in the reaction ^{1}H$(\vec{e}, e'\vec{p})$ [6].

Quantity	Method	Target	Q^2(GeV^2)	Hall	Beam Days
$G_M^{p\ *}$	Elastic scattering	LH_2	7 – 15.5	A	24
G_E^p/G_M^p	Recoil Polarization	LH_2	5 – 12	A	45
G_M^n	$E-p/e-n$ ratio	$LD_2 - LH_2$	3.5 – 13.0	B	30
G_M^n	$E-p/e-n$ ratio	LD_2, LH_2	3.5 – 13.5	A	25
G_E^n/G_M^n	Double polarization asymmetry	polarized ^{3}He	5 – 8	A	50
G_E^n/G_M^n	Recoil Polarization	LD_2	4 – 7	C	50
G_E^n/G_M^n	Recoil Polarization	LD_2	4.5	A	5

Table 1. Listing of approved experiments for measuring the elastic electromagnetic form factors.

This experiment takes advantage of the relationship

$$\frac{G_E^p}{G_M^p} = -\frac{P_t}{P_l}\frac{E+E'}{2M}\tan\left(\frac{\theta_e}{2}\right) \tag{6}$$

where P_t and P_l are the transverse and longitudinal polarizations (measured with a proton polarimeter), E and E' are the electron incident and scattered energies, M is the proton mass, and θ_e is the electron scattering angle. The experiment will rely on the Big Cal lead-glass spectrometer for the electron arm and the new Super BigBite magnetic spectrometer for the proton polarimeter. This experiment has been given a high-impact rating by the JLab PAC and is expected to run in the next 3-4 years. The light blue, filled circles in Figure 2a located on the axis represent the Q^2 values where the measurements will be made and the expected uncertainties. The uncertainties are low and extend out to $Q^2 = 12$ GeV^2. The results could precisely map the location of the zero crossing in the proton form factor ratio where the DSE calculation (recall Figure 4) showed the position of this crossover is sensitive to the shape of the proton mass function $M(p)$. This measurement has the potential to probe a core component of nucleon structure and QCD.

The neutron magnetic form factor G_M^n will be measured in two experiments in Halls A and B. Precise neutron measurements are notoriously difficult so measuring G_M^n with two separate experimental setups provides better control of the systematic uncertainties. The measurement in Hall B (E12-07-104) will use the new CLAS12 detector to extract the ratio R of quasi-elastic (QE) $e-n$ to $e-p$ scattering on deuterium

$$R = \frac{\frac{d\sigma}{d\Omega}[^2\mathrm{H}(e,e'n)_{QE}]}{\frac{d\sigma}{d\Omega}[^2\mathrm{H}(e,e'p)_{QE}]} = a \times \frac{\sigma_{Mott}\left(\frac{(G_E^n)^2+\tau(G_M^n)^2}{1+\tau} + 2\tau\tan^2\frac{\theta_e}{2}(G_M^n)^2\right)}{\frac{d\sigma}{d\Omega}[^1\mathrm{H}(e,e')p]} \tag{7}$$

where a is a nuclear correction [4]. The denominator in Equation 7 is the well-known $e-p$ cross section (whose precision will improve with the G_M^p measurement described above). The numerator contains the desired quantity G_M^n and the neutron electric form factor G_M^n which is small over the range of the G_M^n measurement. Our understanding of G_E^n will be folded into the systematic uncertainty on G_M^n. Using a ratio measurement here reduces the vulnerability to a number of sources of uncertainty (radiative corrections, Fermi motion correction, *etc*). A precise measurement of the neutron detection efficiency (NDE) is required so a dual $LD_2 - LH_2$ target has been proposed to use the $p(e,e'\pi^+n)$ reaction as a source of tagged neutrons to measure NDE at the same time the production data are collected. The systematic uncertainties are expected to be less than 2.5% across the full range out to $Q^2 = 13$ GeV^2. These data will more than double the existing range of precise measurements of G_M^n

as shown by the black points in Figure 1b. The black bar in the figure represents the maximum value of the expected systematic uncertainty.

The second measurement of G_M^n will be performed in Hall A (E12-09-019) [24]. This experiment will also exploit the ratio method on deuterium as in Hall B using the Super BigBite spectrometer for the electron arm and the HCal hadron calorimeter paired with a large bending magnet (BigBen) to separate neutral and charged particles. A separate calibration measurement of the NDE will be made using photons produced by a radiator inserted into the beam and incident on a hydrogen target. The ^{1}H(γ, π^+)n reaction will provide a source of tagged photons and a cut on the pion momentum will select two-body reactions (the end-point method). The expected systematic uncertainties are below 2.1%. The planned Q^2 coverage and uncertainties are represented by the blue, open squares in Figure 1b. The experiment is expected to run in Hall A in the next 2-3 years.

There are also two experiments approved to measure the neutron form factor ratio $\mu_n G_E^n/G_M^n$ in Halls A and C. The Hall A measurement (E12-09-016) will measure a double polarization asymmetry A_{en}^V from $^3\vec{\text{He}}(\vec{e}, e'n)pp$ using a polarized beam and polarized ^{3}He to provide the neutron target [25]. This asymmetry depends on the neutron form factor ratio and a set of known kinematic factors. It is the following

$$A_{en}^V = -\frac{2\sqrt{\tau(\tau+1)}\tan(\theta_e/2)\cos\phi^*\sin\theta^* G_E^n/G_M^n + 2\tau\sqrt{1+\tau+(\tau+1)^2\tan^2(\theta_e/2)}\tan(\theta_e/2)\cos\theta^*}{(G_E^n/G_M^n)^2 + \tau/\epsilon} \tag{8}$$

where θ^* is the polar angle and ϕ^* is the azimuthal angle of the target polarization in the laboratory frame with respect to the axis of the momentum transfer (the other quantities are defined above).

The electron arm will use the Super BigBite spectrometer (same as used in the proton form factor ratio and G_M^n measurements in Hall A) and the HCal hadron calorimeter will detect the scattered neutron (same as used in G_M^n measurement in Hall A). The planned Q^2 coverage and uncertainties are shown as the red, filled squares in Figure 2b. The Q^2 range of the data for this ratio will be extended by nearly a factor of three expanding the opportunity to do a flavor decomposition out to $Q^2 = 10$ GeV^2. These data will challenge the DSE and LFHQCD calculations of Figure 5. The experiment is expected to run in the next 2-3 years.

The second measurement of the neutron form factor ratio is in Hall C (E12-11-009) and is based on the recoil polarization mechanism used for the proton form factor ratio measurement in Hall A (see Equation 6) [26]. In this experiment a deuterium nucleus serves as the neutron target for the ^{2}H$(\vec{e}, e'\vec{n})p$ reaction. The electron is detected in the Super High Momentum Spectrometer and a neutron polarimeter measures the polarization of the scattered neutron. As with the G_M^n measurements, two experiments have been approved for the neutron form factor ratio measurements to provide better understanding of the systematic errors. The Q^2 points and expected uncertainties for this measurement are shown as the blue, filled circles in Figure 2b. At the highest Q^2 point the statistical uncertainties exceed 10% and this method is near the limit of it's applicability. This limit has motivated the last experiment in this report. A short (five days) run has been approved to test the feasibility of using a charge exchange reaction in the neutron polarimeter to expand the reach of the recoil polarization method to higher Q^2 (E12-17-004) [7]. A single point at $Q^2 = 4.5$ GeV^2 will be measured and is shown as the black, filled circle in Figure 2b. This short run is expected in the next 2-3 years while the Hall C neutron ratio method is anticipated after 2020.

4 Summary and Conclusions

In this paper we have discussed the recent gains in our understanding of the fundamental observables the elastic electromagnetic form factors. These studies already have a long history, but new features

have been revealed over the last fifteen years. This new knowledge is built on new technologies in superconducting electron accelerators, high luminosity detectors, and cryogenic and polarized targets. Their application has lead to new discoveries that overturned our previous understanding. Jefferson Lab has a program to measure all of the EEFFs precisely and over a broad kinematic range. This opens the door to extending our understanding of nuclear structure at the quark level (*e.g.* flavor decomposition to extract individual quark form factors) and to stringently challenge our theoretical understanding of QCD with data (*e.g.* distinguish between the DSE approach and the LFHQCD model in Figure 5). This campaign has just begun and we expect much of it to play out in the next few years.

References

[1] R. Hofstadter, H. Fechter, J. McIntyre, Phys. Rev. **91**, 422 (1953)
[2] Nuclear Science Advisory Committee, *The 2015 Long Range Plan for Nuclear Science* (US Department of Energy, 2015)
[3] S. Gilad et al., Experiment E12-07-108, Jefferson Lab, Newport News, VA (2007)
[4] G. Gilfoyle et al., Experiment E12-07-104, Jefferson Lab, Newport News, VA (2007)
[5] V. Punjabi, C.F. Perdrisat, M.K. Jones, E.J. Brash, C.E. Carlson, Eur. Phys. J. **A51**, 79 (2015), 1503.01452
[6] P. Perdrisat et al., Experiment E12-07-109, Jefferson Lab, Newport News, VA (2007)
[7] J. Annand et al., Experiment E12-17-004, Jefferson Lab, Newport News, VA (2017)
[8] A. Puckett et al., Phys. Rev. Lett. **104**, 242301 (2010)
[9] D. Adikaram et al., Phys. Rev. Lett. **114**, 062003 (2015)
[10] G.D. Cates, C.W. de Jager, S. Riordan, B. Wojtsekhowski, Phys. Rev. Lett. **106**, 252003 (2011)
[11] G. Miller, Phys. Rep. **194**, 1 (1990)
[12] I. Cloët et al., Phys. Rev. **C90**, 045202 (2014)
[13] I. Cloët et al., Phys. Rev. Lett. **111**, 101803 (2013)
[14] R. Sufian et al., Phys. Rev. **D95**, 014011 (2017)
[15] J. Segovia, I. Cloët, C. Roberts, S. Schmidt, Few-Body Syst. **55**, 1185 (2014)
[16] J.J. Kelly, Phys. Rev. C **70**, 068202 (2004)
[17] D.J. Wilson, I.C. Cloet, L. Chang, C.D. Roberts, Phys. Rev. **C85**, 025205 (2012), 1112.2212
[18] C. Roberts, **arXiv:1509.02925 [nucl-th]** (2015), 1509.02925
[19] J.J. Dudek, R.G. Edwards, K. Orginos, D.G. Richards, J.Phys.Conf.Ser. **299**, 012007 (2011)
[20] A.W. Thomas, W. Weise, *The Structure of the Nucleon* (Wiley-VCH, 2001)
[21] J.P.A. Committee, Tech. rep., Jefferson Laboratory (2007)
[22] P. Shanahan et al., Phys. Rev. **D90**, 034502 (2014)
[23] M. Diehl, P. Kroll, Eur. Phys. J. C **73**, 2397 (2013)
[24] B. Quinn et al., Experiment E12-09-019, Jefferson Lab, Newport News, VA (2009)
[25] B. Wojtsekhowski et al., Experiment E12-09-016, Jefferson Lab, Newport News, VA (2009)
[26] B. Anderson et al., Experiment E12-11-009, Jefferson Lab, Newport News, VA (2011)